Available online at www.sciencedirect.com
ScienceDirect
International Journal of Heat and Mass Transfer 50 (2007) 1061–1074
International Journal of HEAT and MASS TRANSFER
www.elsevier.com/locate/ijhmt

Interactive free convection from a pair of vertical tube-arrays at moderate Rayleigh numbers

Massimo Corcione *

Dipartimento di Fisica Tecnica, University of Rome "La Sapienza", via Eudossiana 18, Rome 00184, Italy

Received 18 January 2006
Available online 9 January 2007

Abstract

Steady laminar free convection from a pair of vertical arrays of equally-spaced, horizontal isothermal cylinders set in free air, is studied numerically. A specifically developed computer-code based on the SIMPLE-C algorithm is used for the solution of the mass, momentum and energy transfer governing equations. Simulations are performed for pairs of tube-arrays consisting of 1–4 circular cylinders, for center-to-center horizontal and vertical spacings from 1.4 to 24 cylinder-diameters, and from 2 to 12 cylinder-diameters, respectively, and for values of the Rayleigh number based on the cylinder-diameter in the range between 10^2 and 10^4. It is found that any cylinder may exhibit either enhanced or reduced Nusselt numbers with respect to the case of single tube-array, depending on its location in the array, on the geometry of the array, as well as on the Rayleigh number. Heat transfer dimensionless correlating equations are also proposed.

Keywords: Free convection; Vertical arrays of horizontal cylinders; Mutual interactions; Numerical analysis; Correlating equations

1. Introduction

Free convection heat transfer from arrays of horizontal cylinders set in free space has a considerable relevance to several engineering applications, as, e.g., heat exchangers, storage devices, and electronic components. In fact, in many situations, heat transfer designers prefer to avoid the use of mechanical fans or other active equipment for the fluid circulation, due to power consumption, excessive noise, or reliability concerns. Of course, a full understanding of how the buoyant flow fields induced by the individual elements of the array interact, is crucial to evaluate the limits of free convection, which must always be kept in mind.

Despite its practical interest, the investigations conducted on this subject are not so many as might be expected. In addition, most of the papers in this field are substantially oriented toward the study of the thermal performance of the basic configuration represented by the single vertical array of horizontal cylinders [1–7]. A detailed review of these studies is reported in a recent paper by Corcione [8], who performed a numerical investigation of laminar free convection from flat vertical arrays of 2–6 equally-spaced, horizontal isothermal cylinders, for center-to-center separation distances from 2 up to more than 50 cylinder-diameters, and for values of the Rayleigh number based on the cylinder-diameter in the range between 5×10^2 and 5×10^5, with the basic aim to derive heat transfer dimensionless correlating equations for any individual cylinder in the array, and for the whole tube-array.

The first well-documented work on free convection from multiple tube-arrays set in open space was made by Tillman [9], who carried out an experimental study on both square and staggered arrays of electrically-heated cylinders, 1.27 cm in diameter and 10.16 cm long, with same center-to-center horizontal and vertical spacings in the range between 1.43 cm and 3.81 cm, for average cylinder-to-ambient temperature differences in the range between 69 °C and 292 °C. The square arrays consisted of 16

* Tel.: +39 06 44 58 54 43, fax: +39 06 48 80 120.
E-mail address: massimo.corcione@uniroma1.it

0017-9310/$ - see front matter © 2006 Published by Elsevier Ltd.
doi:10.1016/j.ijheatmasstransfer.2006.07.034

Nomenclature

D	diameter of the cylinders
$\mathbf{g}$	gravity vector
g	gravitational acceleration
Gr	Grashof number based on the cylinder-diameter $= g\beta(t_w - r_\infty)D^3/v^2$
H	overall height of the array
k	thermal conductivity of the fluid
N	number of cylinders in any tube-array
N_i	ordinal number of the ith cylinder in the single tube-array
Nu	average Nusselt number of the double tube-array
Nu_0	average Nusselt number of the single tube-array
Nu_i	average Nusselt number of the ith cylinder in the array
$(Nu_i)_0$	average Nusselt number of the ith cylinder in the single tube-array
Nu_s	average Nusselt number of the single cylinder
$Nu_i(\theta)$	local Nusselt number of the ith cylinder in the array
p	dimensionless pressure
Pr	Prandtl number $= v/\alpha$
Q	heat transfer rate
q	heat flux
r	dimensionless radial coordinate
Ra	Rayleigh number based on the cylinder-diameter $= g\beta(t_w - t_\infty)D^3/\alpha v$
S_h	horizontal center-to-center separation distance
S_v	vertical center-to-center separation distance
T	dimensionless temperature
t	temperature
U	dimensionless vertical or radial velocity component
$\mathbf{V}$	dimensionless velocity vector
V	dimensionless horizontal or tangential velocity component
X	dimensionless vertical coordinate
Y	dimensionless horizontal coordinate

Greek symbols

α	thermal diffusivity of the fluid
β	coefficient of volumetric thermal expansion of the fluid
v	kinematic viscosity of the fluid
θ	dimensionless polar coordinate
ρ	density of the fluid

Subscripts

opt	optimum value
w	referred to the cylinder surface
1	referred to the bottom cylinder in the array
∞	referred to the undisturbed fluid

cylinders, whilst 14 cylinders were used for the staggered arrays. The tube spacing was found to have a stronger influence on the heat transfer rate than the arrangement of the array, i.e., square or staggered.

Numerical simulations were successively performed by Farouk and Guceri [10], who conducted a study of laminar and turbulent free convection from single and double, both in-line and staggered, horizontal rows of isothermal cylinders. For a single row of cylinders, solutions were obtained for the Rayleigh number range of 10^3–10^5 whilst the center-to-center horizontal spacing was varied from 2 to 6 cylinder-diameters; moreover, for the closest-spacing configuration, predictions were extended up to $Ra = 10^9$. An optimum spacing for maximum heat transfer rate was found to decrease with increasing the Rayleigh number. For the double rows of cylinders, both the horizontal and the vertical spacings were kept equal to 4 cylinder-diameters, and the solutions were obtained for Rayleigh numbers in the range between 10^3 and 10^5. For the in-line arrangement, the mean Nusselt number for the bottom cylinders was found to be about the same as that for the single row of cylinders, whilst the mean Nusselt number for the top cylinders was found to be higher. In contrast, for the staggered arrangement, the mean Nusselt number for the bottom cylinders was found to have increased compared to the case of a single row of cylinders, whilst the mean Nusselt number for the top cylinders was found to decrease.

Leaving aside the studies related to pin-fin dissipators, which have a bearing on this subject only by a purely qualitative viewpoint, no other significant study expressly dedicated to free convection from unconfined multiple tube-arrays was uncovered by the author in the open literature.

In this framework, the aim of the present paper is to carry out an in-depth investigation on both the nature and the effects of the free convective interactions which occur between a pair of flat vertical arrays of horizontal isothermal cylinders set parallel to each other in free space. The study is performed numerically under the assumption of steady laminar flow, for pairs of tube-arrays consisting of 1–4 circular cylinders, for center-to-center horizontal and vertical spacings from 1.4 to 24 cylinder-diameters, and from 2 to 12 cylinder-diameters, respectively, and for values of the Rayleigh number based on the cylinder-diameter in the range between 10^2 and 10^4.

2. Mathematical formulation

Two vertical tube-arrays, each consisting of N equally-spaced, horizontal circular cylinders of diameter D, are

considered, as sketched in Fig. 1. Both the horizontal and the vertical center-to-center separation distances S_h and S_v are assigned. Free convection heat transfer occurs between the cylinder surfaces, kept at uniform temperature t_w, and the surrounding undisturbed fluid reservoir, assumed at uniform temperature t_∞.

The buoyancy-induced flow is considered to be steady and laminar. The cylinders are assumed to be much longer than their diameter, which implies that the end effects can reasonably be neglected and the temperature and velocity fields can be considered two-dimensional. The fluid is assumed to be incompressible, with constant physical properties and negligible viscous dissipation and pressure work. The buoyancy effects on momentum transfer are taken into account through the Boussinesq approximation.

Once the above assumptions are employed in the conservation equations of mass, momentum, and energy, the following set of dimensionless governing equations is obtained:

$$\nabla \cdot \mathbf{V} = 0 \tag{1}$$

$$(\mathbf{V} \cdot \nabla)\mathbf{V} = -\nabla p + \nabla^2 \mathbf{V} - \frac{Ra}{Pr} T \frac{\mathbf{g}}{g} \tag{2}$$

$$(\mathbf{V} \cdot \nabla) T = \frac{1}{Pr} \nabla^2 T \tag{3}$$

where $\mathbf{V}$ is the velocity vector having dimensionless velocity components U and V normalized with v/D; T is the dimensionless temperature excess over the uniform temperature of the surrounding undisturbed fluid normalized with the temperature difference $(t_w - t_\infty)$; p is the dimensionless pressure normalized with $\rho_\infty v^2/D^2$; $\mathbf{g}$ is the gravity vector; $Ra = g\beta(t_w - t_\infty)D^3/v\alpha$ is the Rayleigh number based on the cylinder-diameter; and $Pr = v/\alpha$ is the Prandtl number.

The related boundary conditions are $T = 1$ and $\mathbf{V} = 0$ at the cylinder surfaces, and $T = 0$ and $\mathbf{V} = 0$ at very large distance from both tube-arrays.

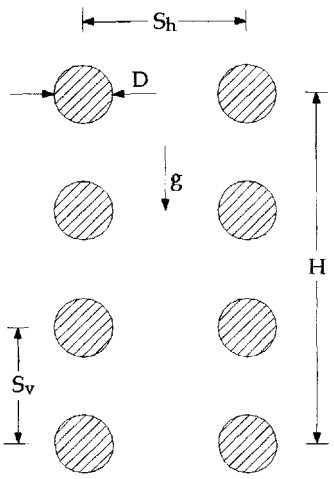

Fig. 1. Sketch of the double tube-array.

3. Discretization grid system

The finite-difference solution of the governing equations (1)–(3) with the proper boundary conditions requires that a discretization grid system is established across the whole integration domain.

Since the flow is symmetric about the vertical plane located midway the tube-arrays, the two-dimensional integration domain is taken as a rectangle which includes only one of the two tube-arrays, i.e., the right tube-array, and extends from the vertical symmetry midline up to a pseudo-boundary line set sufficiently far away from the array. According to the geometry of the system, a cylindrical polar grid is employed in the proximity of each cylinder, whilst a Cartesian grid is used to fill the remainder of the integration domain, as sketched in the left panel of Fig. 2, where the coordinate systems adopted are also represented. The r and θ coordinates of the polar systems are measured from the center of the cylinders, and anti-clockwise from downwards, respectively. In the polar systems, U is the radial velocity component, and V is the tangential velocity component. As concerns the Cartesian system, whose origin is taken at the center of the bottom cylinder, the X-axis is vertical and pointing upwards in the direction opposite to the gravity vector, whereas the Y-axis is horizontal. In this system, U is the vertical velocity component, and V is the horizontal velocity component. According to the discretization scheme originally developed by Launder and Massey [11], the cylindrical polar grids and the Cartesian grid, which are entirely independent of one another, overlap with no attempt of node-matching. Their connection is provided by a row of false nodes, one for each neighboring grid, located beyond their intersection, as depicted in the middle panel of Fig. 2.

4. Boundary conditions

The boundary conditions required for the numerical solution of the governing equations (1)–(3) have to be specified at each of the boundary lines which enclose the two-dimensional integration domain defined above. As regards the outer pseudo-boundary line, once this is placed sufficiently far away from the cylinders, the fluid may reasonably be assumed to enter or leave the integration flow-domain in the direction normal to the boundary line. The entering fluid is assumed at the ambient temperature. For the leaving fluid, whose temperature is not known a priori, a zero temperature gradient normal to the boundary line is assumed, thus implying that the local heat transfer is dominated by convection rather than by conduction, provided that the outflow velocity is sufficiently large.

The following boundary conditions are then applied:

(a) at the left symmetry line A–D

$$\frac{\partial U}{\partial Y} = 0, \quad V = 0, \quad \frac{\partial T}{\partial Y} = 0 \tag{4}$$

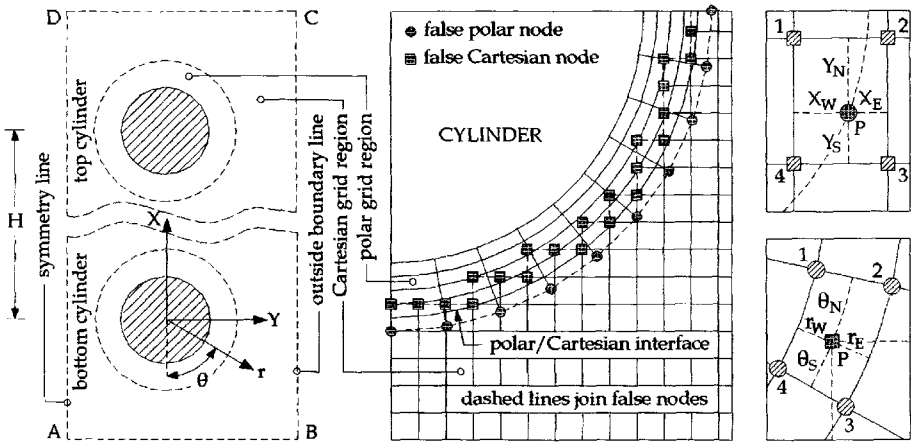

Fig. 2. Sketch of the coordinate systems and of the discretization grid system.

(b) at the cylinder surfaces

$$U = 0, \quad V = 0, \quad T = 1 \tag{5}$$

(c) at the bottom boundary line A–B

$$\frac{\partial U}{\partial X} = 0, \quad V = 0, \quad T = 0 \text{ if } U \geqslant 0 \quad \text{or} \quad \frac{\partial T}{\partial X} = 0 \text{ if } U < 0 \tag{6}$$

(d) at the right boundary line B–C

$$U = 0, \quad \frac{\partial V}{\partial Y} = 0, \quad T = 0 \text{ if } V < 0 \quad \text{or} \quad \frac{\partial T}{\partial Y} = 0 \text{ if } V \geqslant 0 \tag{7}$$

(e) at the top boundary line C–D

$$\frac{\partial U}{\partial X} = 0, \quad V = 0, \quad T = 0 \text{ if } U < 0 \quad \text{or} \quad \frac{\partial T}{\partial X} = 0 \text{ if } U \geqslant 0 \tag{8}$$

Moreover, as far as the intersections between polar and Cartesian grids are concerned, the values of the dependent variables at the false nodes are obtained by a linear interpolation of the values at the four surrounding real nodes. With reference to the symbols denoted in the right panels of Fig. 2, the value of the general dependent variable ϕ at any false Cartesian or polar node is calculated through the following equations, respectively:

$$\phi_P = \frac{\phi_1 X_E Y_S + \phi_2 X_W Y_S + \phi_3 X_W Y_N + \phi_4 X_E Y_N}{(X_W + X_E)(Y_S + Y_N)} \tag{9}$$

$$\phi_P = \frac{\phi_1 r_E \theta_S + \phi_2 r_W \theta_S + \phi_3 r_W \theta_N + \phi_4 r_E \theta_N}{(r_W + r_E)(\theta_S + \theta_N)} \tag{10}$$

5. Solution procedure

The set of governing equations (1)–(3) with the boundary conditions (4)–(10) is solved through a control-volume formulation of the finite-difference method. The pressure–velocity coupling is handled by the SIMPLE-C algorithm by Van Doormaal and Raithby [12], which is essentially a more implicit variant of the SIMPLE algorithm by Patankar and Spalding [13]. The advection fluxes across the surfaces of the control volumes are evaluated by the QUICK discretization scheme by Leonard [14]. Details on the SIMPLE procedure may be found in Patankar [15]. Studies on the comparative performance of different discretization schemes for the evaluation of the interface fluxes, as well as studies on enhanced variants of the SIMPLE algorithm, are widely available and well referenced in the open literature (see, e.g., [16]).

Fine uniform mesh-spacings are used for the discretization of both the polar grid regions and the Cartesian grid region. Starting from specified first-approximation distributions of the dependent variables across the integration domain, the discretized governing equations are solved iteratively through a line-by-line application of the Thomas algorithm. Under-relaxation is used to ensure the convergence of the iterative procedure. The solution is considered to be fully converged when the maximum absolute values of both the mass source and the percent changes of the dependent variables at any grid-node from iteration to iteration are smaller than prescribed values, i.e., 10^{-4} and 10^{-6}, respectively.

After convergence is attained, the local and average Nusselt numbers $Nu_i(\theta)$ and Nu_i of any ith cylinder in the array are calculated

$$Nu_i(\theta) = \frac{qD}{k(t_w - t_\infty)} = \left.\frac{\partial T}{\partial r}\right|_{r=0.5} \tag{11}$$

$$Nu_i = \frac{Q}{\pi k(t_w - t_\infty)} = -\frac{1}{\pi}\int_0^\pi \left.\frac{\partial T}{\partial r}\right|_{r=0.5} d\theta \tag{12}$$

where q is the heat flux and Q is the heat transfer rate. The temperature gradients at the cylinder surfaces are evaluated by assuming a second-order temperature profile among each wall-node and the next two fluid-nodes along the radial direction. The integrals are approximated by the

trapezoid rule. The average Nusselt number of the whole array Nu is then obtained as the arithmetic mean value of the average Nusselt numbers Nu_i of the individual cylinders in the array:

$$Nu = \frac{1}{N}\sum_{i=1}^{N} Nu_i \tag{13}$$

Tests on the dependence of the results obtained on the mesh-spacing of both the polar and the Cartesian discretization grids, as well as on the thickness of the polar grid regions, and on the extent of the whole computational domain, have been performed for a wide variety of geometrical configurations analysed, and of Rayleigh numbers investigated. In particular, the optimal grid-size values, and the optimal positions of the polar/Cartesian interfaces and of the outer pseudo-boundary line, i.e., those used for computations, which represent a good compromise between solution accuracy and computational time required, are assumed as those over which further grid refinements or interface and/or outer boundary-line displacements do not produce noticeable modifications in both the heat transfer rates and the predicted flow field. Namely, when, for each cylinder in the array, the percent changes of the local and average Nusselt numbers $Nu_i(\theta)$ and Nu_i defined above, as well as the percent change of the maximum value of the tangential velocity component at $\theta = 90°$ are smaller than prescribed accuracy values, i.e., 1% and 2%, respectively. Typically: (a) the number of nodal points ($r \times \theta$) of the polar discretization grids lie in the range between 45×72 and 135×90, (b) the thickness of the polar grid regions varies between one-fifth and five times the cylinder-diameter, and (c) the extent of the whole integration flow-domain ranges between 4 and 20 times the cylinder-diameter, depending on the Rayleigh number, as well as on the number of cylinders in the array, and on the horizontal and vertical center-to-center separation distances.

As far as the validation of both the numerical code and the discretization grid scheme is concerned, the local and average Nusselt numbers obtained for a single cylinder at several Rayleigh numbers have been compared with the corresponding benchmark numerical results by Saitoh et al. [17], as shown in Tables 1 and 2, respectively, where other data available in the literature are also reported, i.e., the numerical results by Wang et al. [18], and Kuehn and Goldstein [19], as well as the interpolations of the experimental data by Clemes et al. [20], and the data

Table 1
Comparison of the present solutions for the local Nusselt number of a single cylinder with the benchmark solutions of Saitoh et al. and with the results of Wang et al. and Kuehn and Goldstein

Ra		$Nu_s(\theta)$						
		$\theta = 0°$	30°	60°	90°	120°	150°	180°
10^3	Present	3.789	3.755	3.640	3.376	2.841	1.958	1.210
	Saitoh et al. [17]	3.813	3.772	3.640	3.374	2.866	1.975	1.218
	Wang et al. [18]	3.860	3.820	3.700	3.450	2.930	1.980	1.200
	Kuehn and Goldstein [19]	3.890	3.850	3.720	3.450	2.930	2.010	1.220
10^4	Present	5.986	5.931	5.756	5.406	4.716	3.293	1.532
	Saitoh et al. [17]	5.995	5.935	5.750	5.410	4.764	3.308	1.534
	Wang et al. [18]	6.030	5.980	5.800	5.560	4.870	3.320	1.500
	Kuehn and Goldstein [19]	6.240	6.190	6.010	5.640	4.820	3.140	1.460
10^5	Present	9.694	9.595	9.297	8.749	7.871	5.848	1.989
	Saitoh et al. [17]	9.675	9.577	9.278	8.765	7.946	5.891	1.987
	Wang et al. [18]	9.800	9.690	9.480	8.900	8.000	5.800	1.940
	Kuehn and Goldstein [19]	10.150	10.030	9.650	9.020	7.910	5.290	1.720

Table 2
Comparison of the present solutions for the average Nusselt number of a single cylinder with the benchmark solutions of Saitoh et al. and other data available in the literature

	Nu_s						
	$Ra = 10^2$	5×10^2	10^3	5×10^3	10^4	5×10^4	10^5
Present	1.961	2.634	3.023	4.127	4.819	6.807	7.886
Saitoh et al. num. data [17]	–	–	3.024	–	4.826	–	7.898
Wang et al. num. data [18]	–	–	3.060	–	4.860	–	7.970
Kuehn and Goldstein num. data [19]	2.050	–	3.090	–	4.940	–	8.000
Clemes et al. exp. data [20]	2.070	2.720	3.040	4.190	4.850	6.870	8.030
Morgan eqn. [21]	2.020	2.730	3.110	4.220	4.800	7.180	8.540
Churchill and Chu eqn. [22]	1.599	2.213	2.563	3.655	4.278	6.219	7.327
Raithby and Hollands eqn. [23]	2.100	2.760	3.140	4.300	4.970	7.090	8.330
Kuehn and Goldstein eqn. [24]	2.110	2.770	3.140	4.280	4.920	6.920	8.050

Table 3
Comparison of the present solutions for the average Nusselt number of any individual cylinder in a 2-cylinder vertical array with the experimental results of Tokura et al. at $Gr = 1.2 \times 10^5$

2-Cylinder vertical array at $Gr = 1.2 \times 10^5$		Nu/Nu_s			
		$S_v/D = 1.1$	1.3	1.5	2
Bottom cylinder	Present	0.908	0.965	0.996	1.008
	Tokura et al. [5]	0.890	0.940	1.000	1.010
Top cylinder	Present	0.614	0.661	0.726	0.853
	Tokura et al. [5]	0.610	0.680	0.740	0.870
Whole array	Present	0.761	0.813	0.861	0.930
	Tokura et al. [5]	0.750	0.810	0.870	0.940

Table 4
Comparison of the present solutions for the average Nusselt number of the top cylinder in a 2-cylinder vertical array with the experimental results of Sparrow and Niethammer

Top cylinder of a 2-cylinder vertical array	Nu/Nu ($S_v/D = 2$)		
	$Ra = 2 \times 10^4$	6×10^4	10^5
Present	0.810	0.844	0.856
Sparrow and Niethammer [4]	0.820	0.850	0.860

which can be derived from the correlating equations by Morgan [21], Churchill and Chu [22], Raithby and Hollands [23], and Kuehn and Goldstein [24]. Moreover, in order to test the reliability of the composite polar/Cartesian grid system at close spacing between the cylinders, the results obtained for a two-cylinder vertical array have been compared with the experimental data by Tokura et al. [5] for $Gr = 1.2 \times 10^5$ and S_h/D in the range between 1.1 and 2, and those by Sparrow and Niethammer [4] for $S_h/D = 2$ and Ra in the range between 2×10^4 and 10^5, as shown in Tables 3 and 4, respectively. Additional details on the code validation are available in Ref. [8].

6. Results and discussion

Numerical simulations are performed for $Pr = 0.71$, which corresponds to air, and different values of (a) the Rayleigh number Ra in the range between 10^2 and 10^4, (b) the number N of cylinders of each tube-array in the range between 1 and 4, (c) the horizontal center-to-center dimensionless separation distance S_h/D in the range between 1.4 and 24, and (d) the vertical center-to-center dimensionless separation distance S_v/D in the range between 2 and 12.

The results for pairs of individual cylinders, i.e., for $N = 1$, and those for pairs of cylinder-arrays, i.e., for $N > 1$, will be discussed in two separate sections. The heat transfer results will be presented mainly in relative terms, i.e., in terms of the ratio Nu/Nu_s, for the configurations with $N = 1$, and of the ratios $Nu_i/(Nu_i)_0$ and Nu/Nu_0, for the configurations with $N > 1$, so as to highlight in what measure the convective interactions between the parallel tube-arrays either enhance or degrade the heat transfer rates from any individual cylinder and from the double tube-array as a whole, in comparison with those typical for the single tube-array.

In this context, before proceeding with the discussion of the results, the heat transfer dimensionless correlating equations previously derived in Ref. [8] for the single cylinder, for any individual cylinder in a single vertical tube-array, and for a single vertical tube-array as a whole, are reported for the reader's convenience.

6.1. Résumé of heat transfer dimensionless correlating equations

The average Nusselt number Nu_s of the single cylinder for Rayleigh numbers in the range $10^2 \leqslant Ra \leqslant 10^4$ is expressed as a function of Ra by the following simple algebraic correlation:

$$Nu_s = 0.769 Ra^{0.198} \tag{14}$$

with percent standard deviation of error $E_{sd} = 0.41\%$, and range of error E from -0.92% to $+0.71\%$.

The average Nusselt number $(Nu_i)_0$ of any individual ith cylinder in a single vertical tube-array is correlated to the Rayleigh number Ra, to the cylinder location relative to the center of the bottom cylinder (x/D), and to the ordinal number N_i of the cylinder, by the following two distinct transcendental equations:

$$\begin{aligned} &(Nu_i)_0 = Ra^{0.25}\{3.364 \ln[(x/D)^{0.4}/N_i^{0.9}] + 0.508\}, \\ &2 \leqslant N_i \leqslant 6, \;\; 2(N_i - 1) < x/D \leqslant 8 + N_i, \\ &5 \times 10^2 \leqslant Ra \leqslant 5 \times 10^5 \end{aligned} \tag{15}$$

with percent standard deviation of error $E_{sd} = 3.19\%$, and range of error E from -5.07% to $+7.97\%$;

$$\begin{aligned} &(Nu_i)_0 = Ra^{0.25}\{0.587 \ln[(x/D)^{0.33}/N_i^{0.5}] + 0.350\}, \\ &2 \leqslant N_i \leqslant 6, \;\; 8 + N_i < x/D \leqslant (10^9/Ra)^{0.333}, \\ &5 \times 10^2 \leqslant Ra \leqslant 5 \times 10^5 \end{aligned} \tag{16}$$

with percent standard deviation of error $E_{sd} = 3.27\%$, and range of error E from -5.93% to $+7.96\%$.

The average Nusselt number Nu_0 of the whole single vertical tube-array is correlated to the Rayleigh number Ra, to the cylinder-spacing S_v/D, and to the number N of cylinders in the array, by the following two distinct transcendental equations:

$$\begin{aligned} &Nu_0 = Ra^{0.235}\{0.292 \ln[(S_v/D)^{0.4} \times N^{-0.2}] + 0.447\}, \\ &2 \leqslant N \leqslant 6, \;\; S_v/D \leqslant 10 - \mathrm{Log}(Ra), \\ &5 \times 10^2 \leqslant Ra \leqslant 5 \times 10^5 \end{aligned} \tag{17}$$

with percent standard deviation of error $E_{sd} = 2.25\%$, and range of error E from -4.79% to $+5.27\%$;

$$Nu_0 = Ra^{0.235}\{0.277\ln[(S_v/D)^{0.4} \times N^{0.2}] + 0.335\},$$
$$2 \leqslant N \leqslant 6,\ \ S_v/D > 10 - \mathrm{Log}(Ra),$$
$$5 \times 10^2 \leqslant Ra \leqslant 5 \times 10^5 \qquad (18)$$

with percent standard deviation of error $E_{sd} = 2.72\%$, and range of error E from -6.40% to $+6.09\%$.

It is worth noticing that, according to the results obtained from a set of numerical simulations recently performed for single vertical tube-arrays at Rayleigh numbers 10^2, 2×10^2, and 3.5×10^2, the range of validity of Eqs. (15)–(18) may be extended to 10^2, i.e., the range $5 \times 10^2 \leqslant Ra \leqslant 5 \times 10^5$ may be replaced by $10^2 \leqslant Ra \leqslant 5 \times 10^5$, with same range of percent errors indicated above.

6.2. Heat transfer from a pair of individual cylinders set side by side ($N = 1$)

The heat transfer performance of a pair of individual cylinders set in free air side by side ($N = 1$) is pointed out in Fig. 3, where the distributions of the ratio Nu/Nu_s vs. the horizontal center-to-center dimensionless separation distance S_h/D, are reported for Rayleigh numbers 10^2, 10^3, and 10^4.

As expected, for large cylinder-spacings the average Nusselt number of any cylinder approaches that for a single cylinder. As S_h/D decreases, Nu/Nu_s increases up to a point, and this is due to the increased flow rate drawn between the cylinders by the "chimney effect", which enhances the local heat transfer. The S_h/D value corresponding to the peak of Nu/Nu_s is defined as the optimum cylinder spacing $(S_h/D)_{opt}$. It may be seen that the impact of the "chimney effect" is higher at higher values of the Rayleigh number, and the value of $(S_h/D)_{opt}$ decreases with increasing Ra, which is due to the corresponding decrease of the boundary layer thickness. As S_h/D is further decreased below $(S_h/D)_{opt}$, the joining of the two boundary layers leads to a heat transfer decrease, which becomes very sharp at close spacing. In fact, as the two cylinders are literally embraced by a unique boundary layer, the amount of heat transferred to the quasi-motionless fluid located between them reduces drastically. In addition, the flow configuration downstream of the cylinders no longer resembles two plumes arising from individual cylinders, but a single plume originated by a single source. This reflects the widening of the region of the rear stagnation point for both cylinders, which implies a decrease in the amount of heat exchanged at their upper surface. A detailed close-up for S_h/D in the range between 1.4 and 3 is presented in Fig. 4, where the numerical data obtained for $Ra = 5 \times 10^2$ and 5×10^3 are also reported.

Local results are presented in Fig. 5, where equispaced isotherm lines are plotted for the right cylinder of a pair at, e.g., $Ra = 10^3$ and $S_h/D = 1.4$, 2 (at which the maximum of Nu takes place), and 6. The corresponding polar distributions of the local Nusselt number $Nu(\theta)$ are reported in Fig. 6, where the polar distribution of $Nu_s(\theta)$ for the single cylinder at same Rayleigh number is also shown for comparison. It may be observed that, owing to the mutual interactions occurring between the cylinders, the upper and lower stagnation points of the right (or the left) cylinder rotate counterclockwise (or clockwise) from the vertical plane passing through the axis of the cylinder by an angle θ_r which increases as the cylinder spacing decreases. Moreover, both the enhancement and the degradation of the amount of heat locally transferred to the fluid flowing through the cylinders, which occur respectively at $S_h/D = 2$, due to the "chimney effect", and at $S_h/D = 1.4$, due to the merging of the boundary layers, may clearly be noticed.

All the values obtained for the optimum cylinder spacing $(S_h/D)_{opt}$ may be correlated to the Rayleigh number Ra by the following linear equation, as shown in Fig. 7:

$$(S_h/D)_{opt} = 2.6 - 0.2\mathrm{Log}(Ra) \quad \text{for } 10^2 \leqslant Ra \leqslant 10^4 \qquad (19)$$

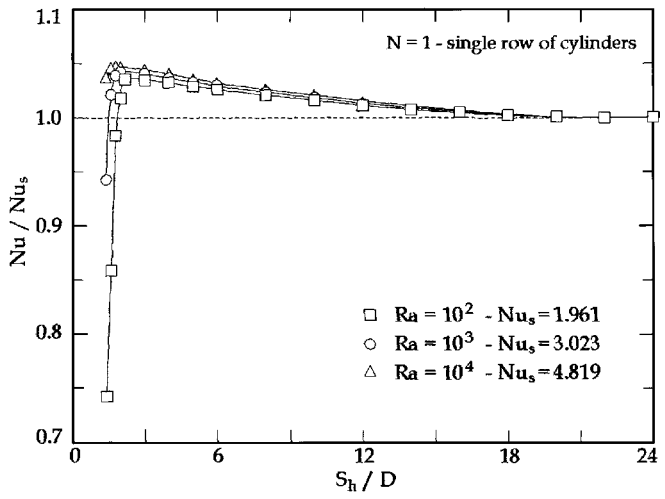

Fig. 3. Distributions of the ratio Nu/Nu_s vs. S_h/D for $N = 1$ and different values of Ra.

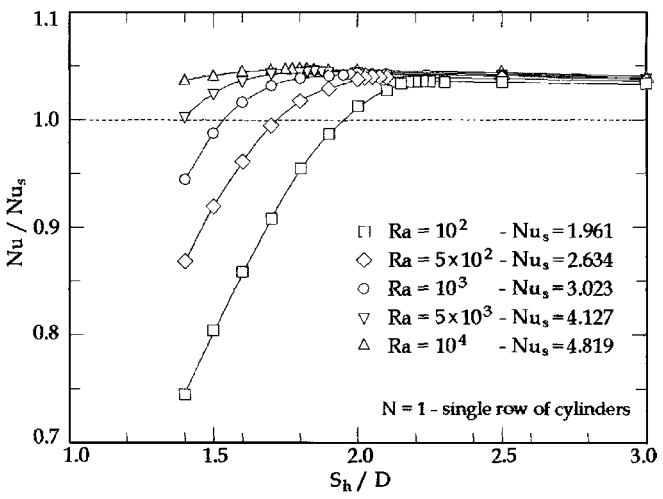

Fig. 4. Close-up of the distributions of Nu/Nu_s vs. S_h/D for $N = 1$ and different values of Ra.

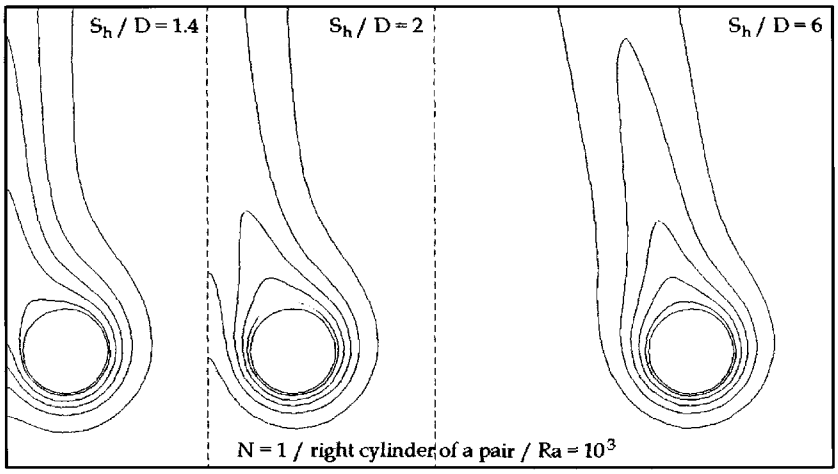

Fig. 5. Isotherm contour plots for the right cylinder of a pair, for $Ra = 10^3$ and different values of S_h/D.

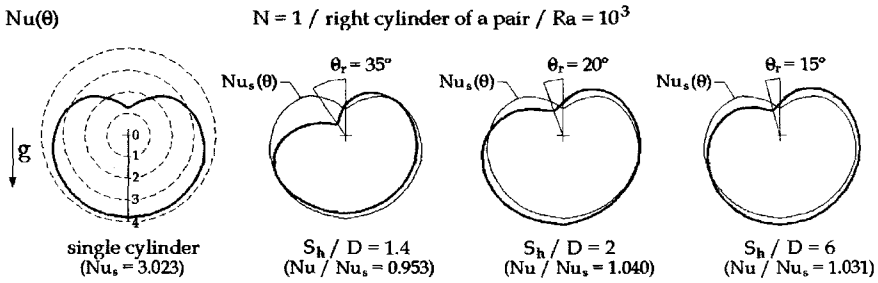

Fig. 6. Polar distributions of $Nu(\theta)$ for the right cylinder of a pair, for $Ra = 10^3$ and different values of S_h/D.

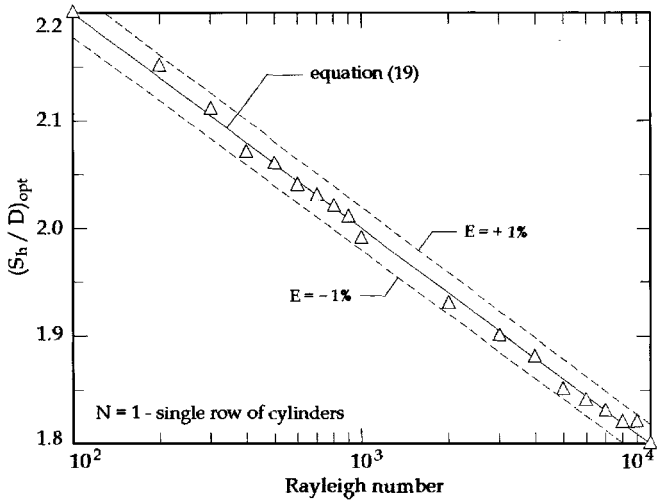

Fig. 7. Distribution of $(S_h/D)_{opt}$ vs. Ra for $N = 1$.

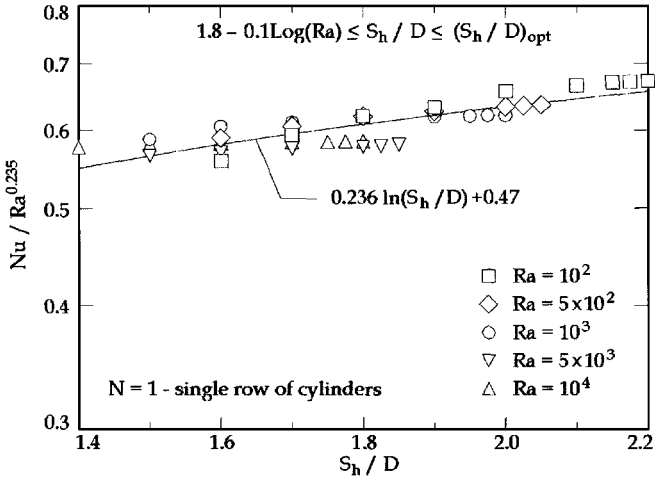

Fig. 8. Comparison between Eq. (20) and the numerical results.

with percent standard deviation of error $E_{sd} = 0.33\%$, and range of error E from -0.27% to $+0.31\%$.

As far as the heat transfer rates are concerned, the numerical results obtained for the average Nusselt number Nu may be correlated to the Rayleigh number Ra, and to the cylinder spacing S_h/D, by the following two distinct transcendental equations, as shown in Figs. 8 and 9:

$$Nu = Ra^{0.235}[0.236\ln(S_h/D) + 0.47],$$
$$1.8 - 0.1\mathrm{Log}(Ra) \leqslant S_h/D \leqslant (S_h/D)_{opt},\ 10^2 \leqslant Ra \leqslant 10^4 \quad (20)$$

with percent standard deviation of error $E_{sd} = 2.85\%$, and range of error E from -4.06% to $+5.15\%$;

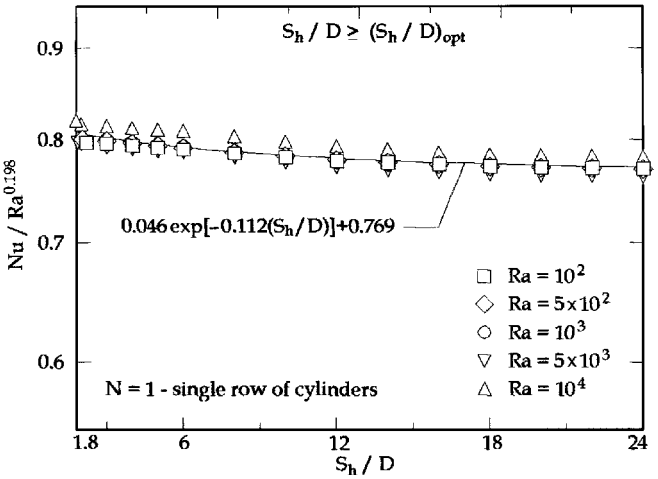

Fig. 9. Comparison between Eq. (21) and the numerical results.

$$Nu = Ra^{0.198}\{0.046\exp[-0.112(S_h/D)] + 0.769\},\quad S_h/D \geqslant (S_h/D)_{opt},\ \ 10^2 \leqslant Ra \leqslant 10^4 \tag{21}$$

with percent standard deviation of error $E_{sd} = 0.68\%$, and range of error E from -1.68% to $+1.00\%$.

6.3. Heat transfer from a pair of vertical tube-arrays set parallel to each other ($N > 1$)

The geometry effects on the average heat transfer rate from the ith of N cylinders are pointed out in Figs. 10–14, where the distributions of the ratio $Nu_i/(Nu_i)_0$ vs. the horizontal dimensionless spacing S_h/D are reported for, e.g., a pair of 3-cylinder tube-arrays ($N = 3$), $Ra = 10^3$, and vertical dimensionless spacings $S_v/D = 2$, 3, 4, 8, and 12, respectively.

As expected, for very large horizontal spacings the average Nusselt number of any ith cylinder of the double tube-array approaches that of the corresponding ith cylinder of a

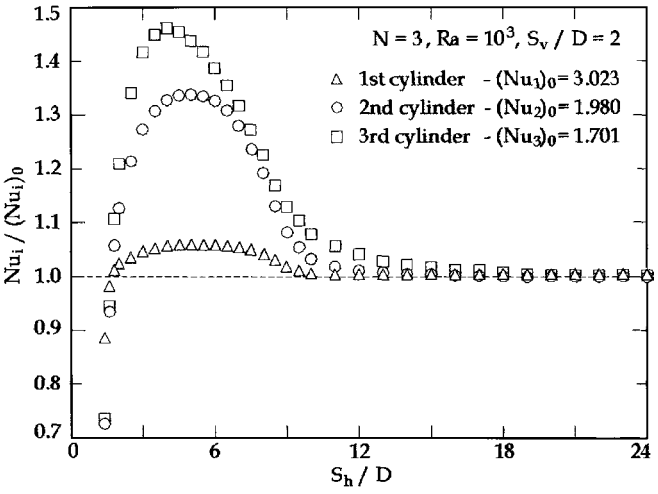

Fig. 10. Distributions of the ratio $Nu_i/(Nu_i)_0$ vs. S_h/D, for $N = 3$, $Ra = 10^3$, and $S_v/D = 2$.

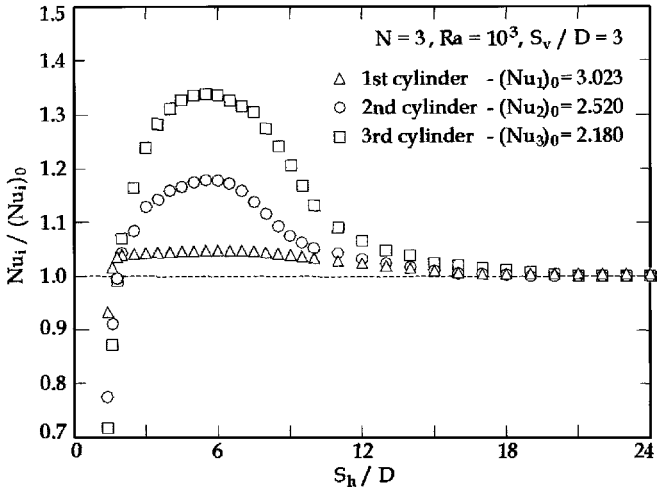

Fig. 11. Distributions of the ratio $Nu_i/(Nu_i)_0$ vs. S_h/D, for $N = 3$, $Ra = 10^3$, and $S_v/D = 3$.

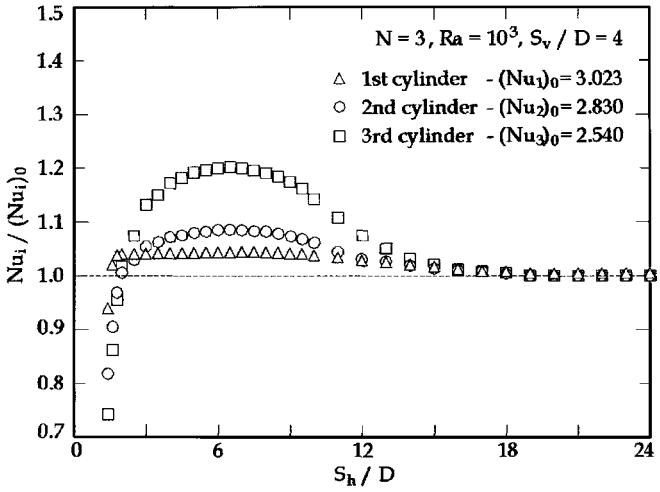

Fig. 12. Distributions of the ratio $Nu_i/(Nu_i)_0$ vs. S_h/D, for $N = 3$, $Ra = 10^3$, and $S_v/D = 4$.

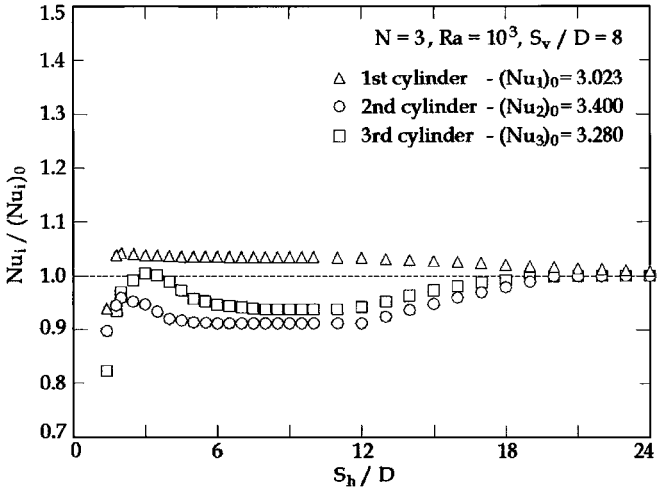

Fig. 13. Distributions of the ratio $Nu_i/(Nu_i)_0$ vs. S_h/D, for $N = 3$, $Ra = 10^3$, and $S_v/D = 8$.

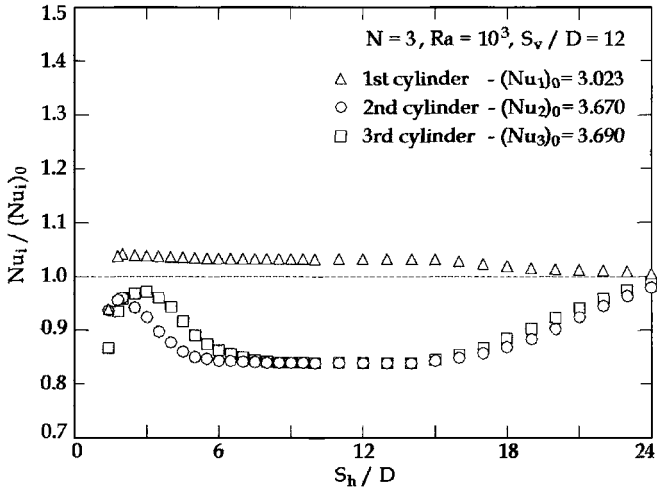

Fig. 14. Distributions of the ratio $Nu_i/(Nu_i)_0$ vs. S_h/D, for $N = 3$, $Ra = 10^3$, and $S_v/D = 12$.

single tube-array, whatever is the vertical spacing between the cylinders. As S_h/D decreases, the distribution of $Nu_i/(Nu_i)_0$ for the bottom cylinder is the same type as that found for a pair of individual cylinders set side by side, i.e., a slight increase up to a point, attributable to the "chimney effect", and a successive sharp decrease, due to the merging of the boundary layers. This same general trend is typical also for the downstream cylinders, but only at small vertical spacings. In fact, at large vertical spacings, $Nu_i/(Nu_i)_0$ decreases from unity with decreasing S_h/D, up to reaching a plateau of relative minimum. As the horizontal spacing is further decreased, the general trend discussed above is restored, i.e., $Nu_i/(Nu_i)_0$ increases up to a maximum, and then decreases steeply at close horizontal spacing. It is interesting to note that at the largest values of S_v/D investigated, the maximum for $Nu_i/(Nu_i)_0$ may remain below unity, which means that the relative heat transfer performance undergoes a degradation at any value of S_h/D.

In order to explain the effects of S_v/D on $Nu_i(Nu_i)_0$ for the downstream cylinders, it is necessary to recall briefly the main heat transfer features of any individual cylinder in a single tube-array. First of all, the heat transfer rate at the bottom cylinder is substantially identical to that for a single cylinder, at least for $S_v/D \geqslant 2$. Secondly, the heat transfer rate at any downstream cylinder may either degrade or enhance with respect to that for a single cylinder, depending on the vertical spacing between the cylinders. In particular, at close cylinder-spacings, degradation is generally the rule, whilst, at large separation distances, enhancement usually predominates. This is a strict consequence of the two opposite effects which originate from the impingement of the warm plume spawned by the preceding cylinder. In fact, the buoyant flow from the upstream cylinder acts as a forced convection field in which the downstream cylinder is embedded. On the other hand, such buoyant flow causes a decrease in the temperature difference between the surface of the downstream cylinder and the adjacent fluid. The first effect, which tends to increase the heat transfer rate at the downstream cylinder, prevails at large spacings. The second effect, which tends to decrease the heat transfer rate at the downstream cylinder, is of major importance at close spacings. A much more detailed discussion may be found in Ref. [8].

When a pair of vertical tube-arrays is considered, the "chimney effect" which arises between them drives an increased airflow rate between the two arrays, vertically through the horizontal spacing between the bottom cylinders, and horizontally through the cylinder-to-cylinder vertical gaps. As a consequence of such horizontal air penetration, the warm plume spawned by any cylinder rotates toward the inside of the double tube-array, and no longer impinges upon the cylinder located downstream in the array. The increase in airflow rate tends to enhance the amount of heat exchanged by any ith cylinder with respect to that exchanged by the corresponding ith cylinder of a single array, whatever is the vertical spacing. On the other hand, the plume rotation toward the inside of the tube bundle may tend to either enhance or degrade the heat transfer performance of any downstream cylinder, depending on the vertical spacing. Enhancement is typical of small vertical spacings, at which any ith downstream cylinder of a single array is affected unfavourably by the impingement of the plume generated by the preceding cylinder. Degradation predominates at large vertical spacings, at which any ith downstream cylinder of a single array is affected positively by the impingement of the plume spawned by the upstream cylinder.

Thus, at close vertical spacings, the positive effects produced by the increased airflow rate, and by the plume rotation, sum up. In contrast, as S_v/D increases, the positive effect produced by the increased airflow rate is progressively counterbalanced by the negative effect caused by the plume rotation, up to being definitely exceeded at the largest vertical spacings investigated. However, since at close horizontal spacing the plume rotation toward the inside of the tube bundle decreases considerably with decreasing S_h/D, the simultaneously renewed effect of the increased airflow rate gives rise to a more or less pronounced peak for $Nu_i/(Nu_i)_0$ also for array-configurations with large values of S_v/D.

The effects of the Rayleigh number on the average heat transfer rate from, e.g., the second cylinder ($i = 2$) of a 3-cylinder configuration ($N = 3$), are shown in Fig. 15, where the distributions of the ratio $Nu_2/(Nu_2)_0$ vs. the Rayleigh number Ra are depicted for $S_h/D = 3$, and vertical spacings $S_v/D = 2$, 3, 4, 8, and 12.

The same type of distributions represented in Figs. 10–14 may be observed, according to the S_v/D value, which means that the effect of the decrease of the Rayleigh number on the relative heat transfer performance is the same as the effect of the decrease of the dimensionless horizontal spacing. In fact, by the convective interactions viewpoint, what essentially matters is the value of the ratio S_h/δ between the center-to-center horizontal spacing and the

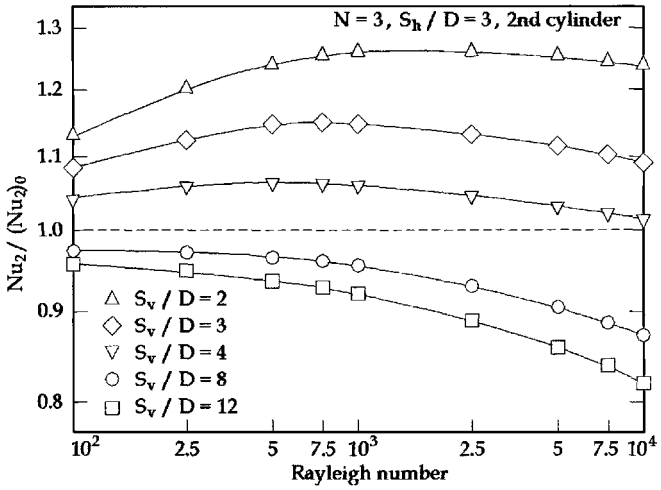

Fig. 15. Distributions of the ratio $Nu_2/(Nu_2)_0$ vs. Ra for the second cylinder of a 3-cylinder double array with $S_h/D = 3$, for different values of S_v/D.

thickness of the boundary layer, as already discussed in the previous section of the paper for $N = 1$. In this context, as Ra is decreased at constant S_h/D, the dimensionless thickness of the boundary layer δ/D increases, and then the ratio S_h/δ decreases, which is exactly what happens if S_h/D is decreased at constant Ra.

Finally, the effects of the number N of cylinders on the amount of heat transferred at the ith cylinder surface are shown in Fig. 16, where the distributions of the ratio Nu_i/Nu_1, and of the ratio $Nu_i/(Nu_i)_0$ along double tube-arrays, each consisting of two to four cylinders, are reported for $Ra = 10^3$, $S_h/D = 2$ and 3, and $S_v/D = 2$ and 3.

It may be noticed that when at least one of the two cylinder-spacings S_h, and S_v is larger than 2 cylinder-diameters, the average heat transfer rate at the ith cylinder is practically independent of the number of downstream cylinders, which permits to assume the problem as a *one-way coordinate problem*. In contrast, for configurations with $S_h/D = 2$ and $S_v/D = 2$, a slight increase in the amount of heat transferred at the ith cylinder surface occurs whenever $i = N$, i.e., in all those cases the ith cylinder is the top cylinder of the array. In fact, at close horizontal and vertical spacings, the fresh air inflow from the outside is quite small due to the pronounced resistance to the flow through the gaps between the cylinders. As a consequence, the region of the rear stagnation point of the top cylinder of each tube-array is smaller than the corresponding region of any other downstream cylinder, thus implying that a larger amount of heat is transferred at its upper surface. Moreover, it is worth observing that, for any ith downstream cylinder, the Nu_i/Nu_1 value enhances, and the $Nu_i/(Nu_i)_0$ value degrades, as S_v/D is increased at constant S_h/D.

The effects of the tube bundle geometry, of the Rayleigh number, and of the number of cylinders on the average heat transfer performance of the whole cylinder-array are now illustrated.

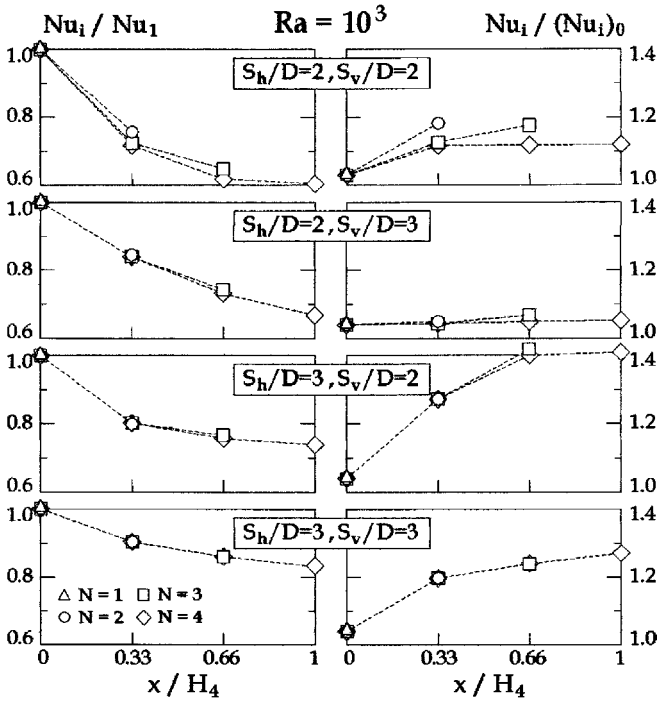

Fig. 16. Distributions of the ratio Nu_i/Nu_1 and $Nu_i/(Nu_i)_0$ through tube-arrays of 2–4 cylinders, for $Ra = 10^3$ and different pairs of values of S_h/D and S_v/D.

The distributions of the ratio Nu/Nu_0 vs. the center-to-center horizontal dimensionless spacing S_h/D for $Ra = 10^3$ and $N = 3$, vs. the Rayleigh number Ra for $S_h/D = 3$ and $N = 3$, and vs. the number N of cylinders for $S_h/D = 3$ and $Ra = 10^3$, are reported in Figs. 17–19, respectively, for different values of the vertical center-to-center dimensionless spacings S_v/D in the range between 2 and 12. Obviously, as both Nu and Nu_0 are simple arithmetic means of the average Nusselt numbers of the individual cylinders in the array, the same types of functional dependencies found for the relative heat transfer performance of any individual

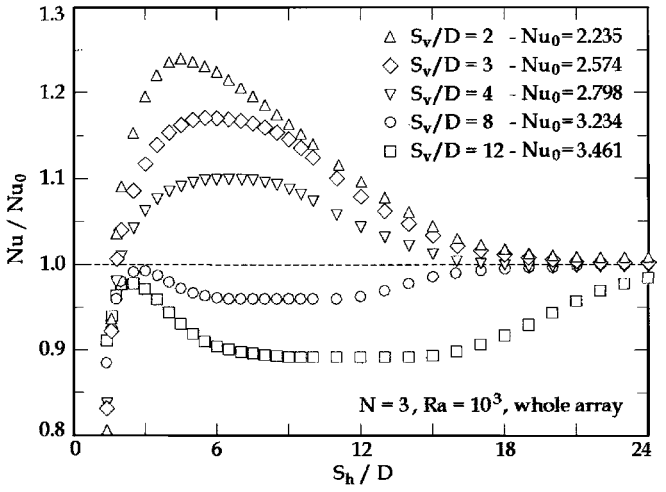

Fig. 17. Distributions of the ratio Nu/Nu_0 vs. S_h/D, for $N = 3$, $Ra = 10^3$, and different values of S_v/D.

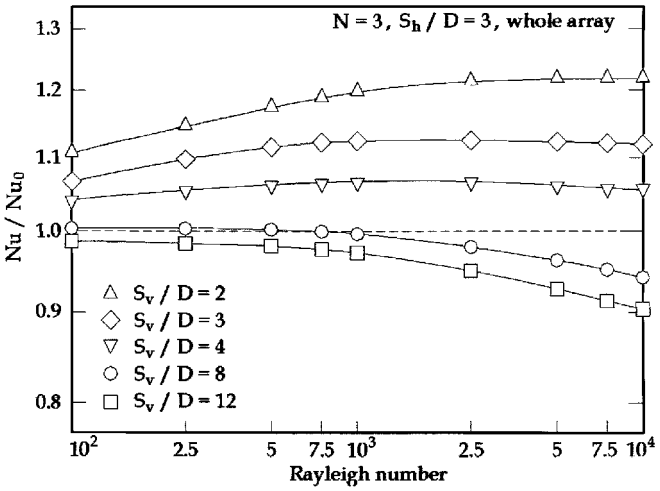

Fig. 18. Distributions of the ratio Nu/Nu_0 vs. Ra, for $N = 3$, S_h/D, and different values of S_v/D.

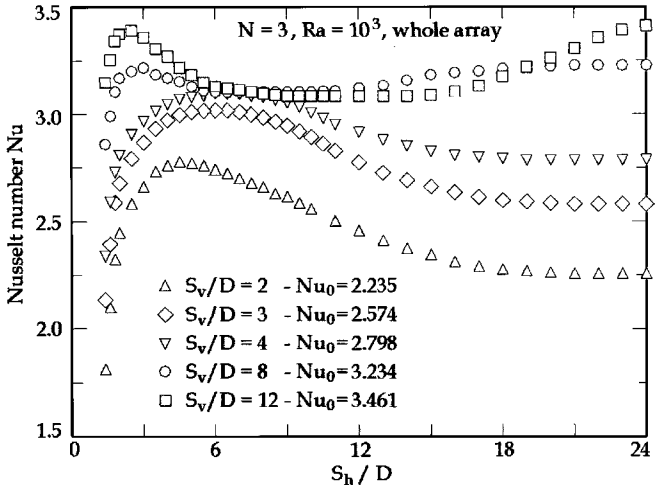

Fig. 20. Distributions of Nu vs. S_h/D, for $N = 3$, $Ra = 10^3$, and different values of S_v/D.

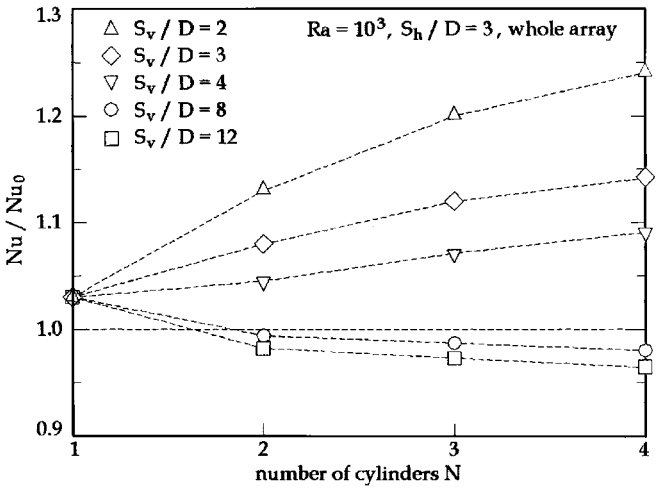

Fig. 19. Distributions of the ratio Nu/Nu_0 vs. N for $Ra = 10^3$, $S_h/D = 3$, and different values of S_v/D.

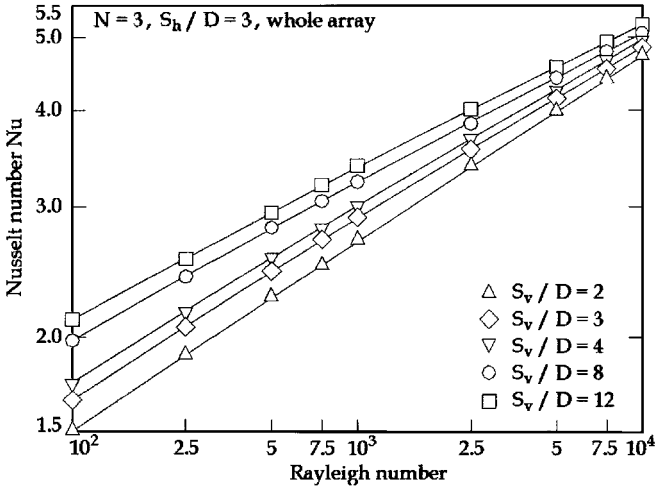

Fig. 21. Distributions of Nu vs. Ra for $N = 3$, $S_v/D = 3$, and different values of S_h/D.

cylinder in the array, represented and discussed in Figs. 10–16, can be observed.

As far as the absolute thermal performance is concerned, the distributions of Nu vs. S_h/D, Ra, and N, for different values of S_v/D, are plotted in Figs. 20–22, respectively. As expected, the average Nusselt number of the whole tube-array increases with increasing the Rayleigh number. In addition, as long as the vertical spacing is kept relatively small, Nu increases with S_h/D, up to reaching a peak at an optimum horizontal spacing $(S_h/D)_{opt}$ which increases with increasing S_v/D. Finally, as long as the horizontal spacing is kept relatively small, Nu either decreases or increases as N increases, according as the vertical spacing is small or large, respectively.

With specific reference to relatively compact configurations, which are undoubtedly the most attractive by the engineering design viewpoint, the numerical results

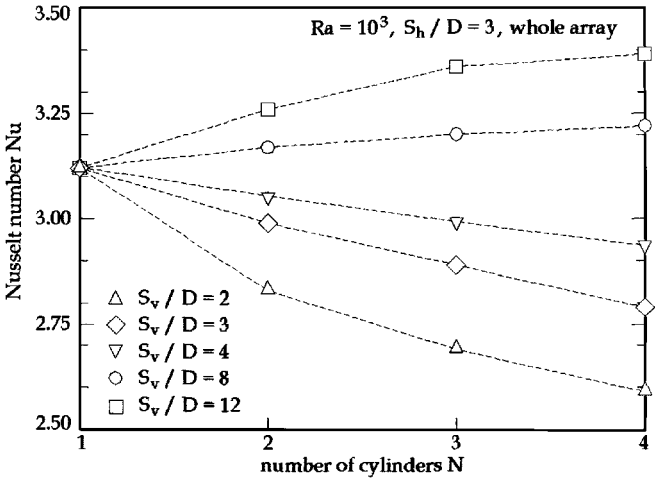

Fig. 22. Distributions of Nu vs. N for $Ra = 10^3$, $S_h/D = 3$, and different values of S_v/D.

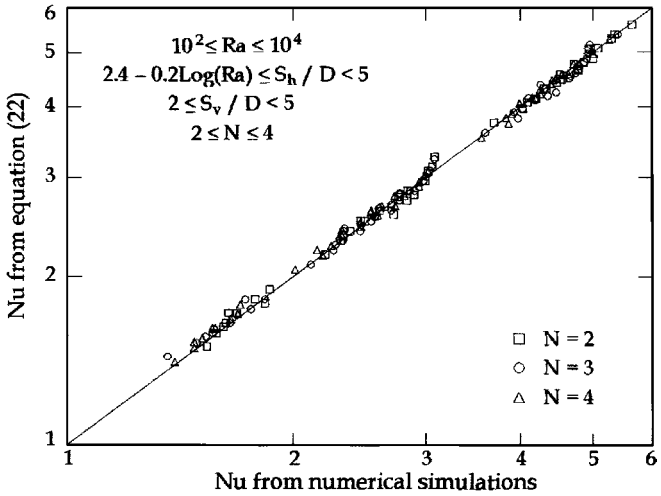

Fig. 23. Comparison between Eq. (22) and the numerical results.

obtained for the average Nusselt number of the double tube-array Nu may be correlated to the Rayleigh number Ra, to the cylinder-spacings S_h/D and S_v/D, and to the number N of cylinders in each vertical tube-array of the pair, by the following algebraic relation, as shown in Fig. 23:

$$Nu = 0.43Ra^{0.235}(S_h/D)^{0.14}(S_v/D)^{0.2}N^{-0.1},$$
$$2 \leqslant N \leqslant 4,\ \ 2.4 - 0.2\mathrm{Log}(Ra) \leqslant S_h/D < 5,$$
$$2 \leqslant S_v/D < 5,\ \ 10^2 \leqslant Ra \leqslant 10^4 \qquad (22)$$

with percent standard deviation of error $E_{sd} = 2.12\%$, and range of error E from -5.32% to $+5.67\%$.

7. Conclusions

Steady laminar free convection from a pair of vertical arrays of equally-spaced, horizontal isothermal cylinders set in free air, has been studied numerically through a specifically developed computer-code based on the SIMPLE-C algorithm. Simulations have been performed for pairs of tube-arrays of 1–4 circular cylinders, for center-to-center horizontal and vertical separation distances from 1.4 to 24 cylinder-diameters, and from 2 to 12 cylinder-diameters, respectively, and for values of the Rayleigh number based on the cylinder-diameter in the range between 10^2 and 10^4. Heat transfer dimensionless correlating equations with rather acceptable standard deviations and absolute value of the maximum relative error, have been proposed.

The main results obtained for pairs of individual cylinders set side by side are:

(a) As S_h/D is decreased from very large values at which the average Nusselt number Nu of any cylinder is the same as that for the single cylinder Nu_s, a "chimney effect" arises between the cylinders. This produces a non negligible increase of Nu/Nu_s up to a peak, which occurs at an optimum horizontal spacing $(S_h/D)_{opt}$. As S_h/D is further decreased below the optimum value, a dramatic degradation of the heat transfer performance takes place owing to the merging of the two boundary layers.
(b) The degree of enhancement of the heat transfer performance Nu/Nu_s increases with increasing the Rayleigh number.
(c) The $(S_h/D)_{opt}$ value decreases with increasing the Rayleigh number.

The main results obtained for pairs of vertical tube-arrays set parallel to each other may be summarized as follows:

(a) The distributions of $Nu_i/(Nu_i)_0$ vs. S_h/D for the bottom cylinders of the double tube-array, as well as for any downstream cylinder at the smaller vertical spacings, is the same type as that found for a pair of individual cylinders set side by side.
(b) In contrast, at the largest vertical spacings, $Nu_i/(Nu_i)_0$ decreases from unity with decreasing S_h/D, up to reaching a plateau of relative minimum. As S_h/D is further decreased, a peak for $Nu_i/(Nu_i)_0$ is detected. However, in many cases, such maximum remains below unity.
(c) Same types of distributions described above are detected for $Nu_i/(Nu_i)_0$ vs. Ra, again depending on the vertical spacing between the cylinders.
(d) The value of $Nu_i/(Nu_i)_0$ either increases or decreases with elevation in the array, according as the vertical spacing is small or large.
(e) When at least one of the two cylinder-spacings S_h and S_v, is larger than 2 cylinder-diameters, the heat transfer rate at the ith cylinder is practically independent of the number of downstream cylinders.
(f) The amount of heat exchanged by the whole double tube-array increases with increasing Ra; in addition, for relatively compact geometries, i.e., for $S_h/D < 5$ and $S_v/D < 5$, Nu increases as both S_h/D and S_v/D increase, whilst decreasing with increasing N.

References

[1] E.R.G. Eckert, E.E. Soehngen, Studies on heat transfer in laminar free convection with the Zehnder-Mach interferometer, AF Technical Report, 5747, U.S.A.F. Air Material Command, Wright–Paterson Air Force Base, Ohio, 1948.
[2] J. Lieberman, B. Gebhart, Interaction in natural convection from an array of heated elements, experimental, Int. J. Heat Mass Transfer 12 (1969) 1385–1396.
[3] G.F. Marsters, Arrays of heated horizontal cylinders in natural convection, Int. J. Heat Mass Transfer 15 (1972) 921–933.
[4] E.M. Sparrow, J.E. Niethammer, Effect of vertical separation distance and cylinder-to-cylinder temperature imbalance on natural convection for a pair of horizontal cylinders, J. Heat Transfer 103 (1981) 638–644.
[5] I. Tokura, H. Saito, K. Kisinami, K. Muramoto, An experimental study of free convection heat transfer from a horizontal cylinder in a vertical array set in free space between parallel walls, J. Heat Transfer 105 (1983) 102–107.

[6] M. Sadegh Sadeghipour, M. Asheghi, Free convection heat transfer from arrays of vertically separated horizontal cylinders at low Rayleigh numbers, Int. J. Heat Mass Transfer 37 (1994) 103–109.
[7] R. Chouikh, A. Guizani, M. Maalej, A. Belghith, Numerical study of the laminar natural convection flow around an array of two horizontal isothermal cylinders, Int. Commun. Heat Mass Transfer 26 (1999) 329–338.
[8] M. Corcione, Correlating equations for free convection heat transfer from horizontal isothermal cylinders set in a vertical array, Int. J. Heat Mass Transfer 48 (2005) 3660–3763.
[9] E.S. Tillman, Natural convection heat transfer from horizontal tube bundles, ASME paper no. 76-HT-35, 1976.
[10] B. Farouk, S.I. Guceri, Natural convection from horizontal cylinders in interacting flow fields, Int. J. Heat Mass Transfer 26 (1983) 231–243.
[11] B.E. Launder, T.H. Massey, The numerical prediction of viscous flow and heat transfer in tube banks, J. Heat Transfer 100 (1978) 565–571.
[12] J.P. Van Doormaal, G.D. Raithby, Enhancements of the simple method for predicting incompressible fluid flows, Numer. Heat Transfer 11 (1984) 147–163.
[13] S.V. Patankar, D.B. Spalding, A calculation procedure for heat, mass and momentum transfer in three-dimensional parabolic flows, Int. J. Heat Mass Transfer 15 (1972) 1787–1797.
[14] B.P. Leonard, A stable and accurate convective modelling procedure based on quadratic upstream interpolation, Comput. Methods Appl. Mech. Engng. 19 (1979) 59–78.
[15] S.V. Patankar, Numerical Heat Transfer and Fluid Flow, Hemisphere Publ. Co., Washington, DC, 1980.
[16] S.V. Patankar, Recent developments in computational heat transfer, J. Heat Transfer 110 (1988) 1037–1045.
[17] T. Saitoh, T. Sajiki, K. Maruhara, Bench mark solutions to natural convection heat transfer problem around a horizontal circular cylinder, Int. J. Heat Mass Transfer 36 (1993) 1251–1259.
[18] P. Wang, R. Kahawita, T.H. Nguyen, Numerical computation of the natural convection flow about a horizontal cylinder using splines, Numer. Heat Transfer 17 (1990) 191–215.
[19] T.H. Kuehn, R.J. Goldstein, Numerical solution to the Navier–Stokes equations for laminar natural convection about a horizontal isothermal circular cylinder, Int. J. Heat Mass Transfer 23 (1980) 971–979.
[20] B. Clemes, K.G.T. Hollands, A.P. Brunger, Natural convection heat transfer from long horizontal isothermal cylinders, J. Heat Transfer 116 (1994) 96–104.
[21] V.T. Morgan, The overall convective heat transfer from smooth circular cylinders, Adv. Heat Transfer 11 (1975) 199–264.
[22] S.W. Churchill, H.H.S. Chu, Correlating equations for laminar and turbulent free convection from a horizontal cylinder, Int. J. Heat Mass Transfer 18 (1975) 1049–1053.
[23] G.D. Raithby, K.G.T. Hollands, Laminar and turbulent free convection from elliptic cylinders with a vertical plate and horizontal circular cylinder as special cases, J. Heat Transfer 98 (1976) 72–80.
[24] T.H. Kuehn, R.J. Goldstein, Correlating equations for natural convection heat transfer between horizontal circular cylinders, Int. J. Heat Mass Transfer 19 (1976) 1127–1134.